Synergetic Effect of Graphene Sheet and Three-Dimensional Crumpled Graphene on the Performance of Dye-Sensitized Solar Cells

Ki-Min Roh, Sun Kyung Kim, and Ji-Hyuk Choi
Rare Metals Research Center, Korea Institute of Geoscience and Mineral Resources, Daejeon 305-350, Republic of Korea

Eun-Hee Jo, Hankwon Chang, and Hee Dong Jang
Rare Metals Research Center, Korea Institute of Geoscience and Mineral Resources, Daejeon 305-350, Republic of Korea

Nanomaterials Science and Engineering Major, University of Science and Technology, Daejeon 305-350, Republic of Korea

DOI 10.1002/aic.15089
Published online November 13, 2015 in Wiley Online Library (wileyonlinelibrary.com)

Herein, an improved structure of the dye-sensitized solar cell (DSSC) is demonstrated which is composed of surface modified fluorine-doped tin oxide (FTO) glass with graphene (GR) sheets and TiO_2 films incorporated with three-dimensional crumped graphene (3-D CGR)/GR sheets. The morphologies of the as-prepared GR sheets on FTO glasses and 3-D CGR/GR sheets/TiO_2 films were observed by field-emission scanning electron microscopy. Light harvesting and charge recombination kinetics were investigated with a solar simulator and electrochemical impedance spectroscopy analysis. In addition to the reduced charge resistance by the GR modified FTO, the enhanced dye loading capability of the 3-D CGR, and the rapid charge transport by the 2-D GR sheets, the power conversion efficiency was 7.2%, which was an increase of 56% compared to a "conventional" structured DSSC. © 2015 American Institute of Chemical Engineers *AIChE J*, 62: 574–579, 2016
Keywords: dye-sensitized solar cell, crumpled graphene, graphene sheet, modification, photoanode

Introduction

Because dye-sensitized solar cells (DSSCs) are considered as an alternative device to traditional silicon-based solar cells due to their low production cost and high conversion efficiency, they have attracted considerable interest from academic fields and industry.[1–3] The typical structure of a DSSC consists of mesoporous TiO_2 photoanode covered with light-absorbing dye molecules, redox-active liquid electrolyte (iodide/tri-iodide based), Pt counterelectrode, and a conducting fluorine-doped tin oxide (FTO) glass.[1] Under light absorption, the excited electrons are injected from the dye molecules into the conduction band of TiO_2 and subsequently transported to the counterelectrode. Therefore, one of the key considerations in enhancing the performance of a DSSC is how many photogenerated electrons can be transported to the collecting electrode while competing with the charge-hole recombination. Because DSSC uses several materials mentioned above, photogenerated electrons must overcome the various interfaces and grain boundaries between the components.[4]

To reduce charge-hole recombination and improve the transport, there are several strategies including (1) additional coatings on the FTO glass[5–7] and (2) introducing electrode materials to heighten the dye adsorption and carrier transport abilities.[4,8] Recently, extensive studies have been carried out to achieve a high conversion efficiency of DSSCs through surface modification of the photoelecrtrode and counterelectrode with graphene.[9–11] Because graphene (GR), a two-dimensional (2-D) carbon nanomaterial with a honeycomb lattice, shows astonishing advantages in device applications due to its remarkable electrical conductivity, high specific surface area, and transparency, it has drawn much attention for enhancing the performance of photovoltaic cells.[12–14] In a previous study, we reported that the surface coating of graphene sheets on FTO glass using the Langmuir–Blodgett (LB) technique could improve the performance of DSSCs by reducing the charge recombination at the TiO_2/FTO interfaces.[15,16] However, this enhancement of the cell performance was not accompanied by an improvement in the TiO_2 photoanode. To obtain a high electron transfer efficiency that was limited by the resistance of the photoanode in DSSCs, we then fabricated a TiO_2 photoanode incorporated with 3-D crumpled graphene (3-D CGR).[17] The 3-D CGR powder synthesized with an aerosol

Additional Supporting Information may be found in the online version of this article.

Ki-Min Roh and Eun-Hee Jo equally contributed to this work as the first author.

Correspondence concerning this article should be addressed to H. D. Jang at hdjang@kigam.re.kr.

spray pyrolysis process showed excellent resistance to restacking or aggregation compared to the easily stacked flat graphene sheets because of their uneven surface.[18,19] As a result, the 3-D CGR powder had a higher specific surface area and adsorbed more dye molecules to produce photogenerated electrons in the photoanode of DSSCs compared to the GR sheets.

Herein, we introduce an improved structure for the DSSC which is composed of a surface modified FTO glass with graphene sheets and 3-D CGR incorporated TiO_2 films to enhance the efficiency of the DSSCs. In addition, we also incorporated the graphene sheets into the TiO_2/3-D CGR nanostructure film to form graphene bridges for the charge transport between the structured materials in the DSSC. This composite photoanode is expected to not only adsorb more dye molecules but also provide additional transport path ways for electrons, leading to a higher conversion efficiency than that of conventional TiO_2-based devices. The morphologies of the as-prepared GR sheets on the FTO glasses and the 3-D CGR/GR sheets/TiO_2 paste were investigated by field-emission scanning electron microscopy (FESEM). Light harvesting and charge recombination kinetics were characterized using a solar simulator and electrochemical impedance spectroscopy (EIS) analysis.

Experimental Procedures

We prepared the colloidal graphene oxide (GO) solution by a modified Hummers' method.[24] Graphite (Alfa Aesar, UCP-1 grade), H_2SO_4, and $K_2S_2O_8$ were mixed together in an 80°C oil bath for the preoxidation process. After the mixing, $KMnO_4$ was slowly added in a 30°C oil bath for the oxidation process. This solution was transferred to an ice bath and a thick paste was formed. Next, we added the distilled water and stirred the solution for 30 min while the temperature was maintained below 50°C. Finally, H_2O_2 was slowly added into the solution. The colloidal mixture was filtered, washed with distilled water, and the filter cake was formed by drying. The dried cake was dispersed in distilled water for 24 h. Then, the supernatant was diluted with 1:5 = distilled water/methanol solution and redispersed by an ultrasonic bath for the LB experiment. In this study, the GO sheets were transferred to the FTO glass at a surface pressure of 20 mN/m, which showed the maximum power conversion efficiency (PCE) of the DSSC. After GO sheets were transferred to the FTO glass, they were dried at room temperature for 3 h and reduced to graphene after annealing at the temperature of 400°C for 3 h.[15]

For the synthesis of the 3-D CGR particles, a colloidal solution as an aerosol precursor was prepared by dispersing the as-prepared GO colloids into 100 mL of deionized water. The concentration of the GO was fixed at 0.1 wt %. GO sheets in the colloidal solution were exfoliated by ultrasonic treatment for 1 h 20 min before the aerosol spray pyrolysis process. A description of the experimental procedure used for the aerosol process is available in the literature.[20,21] The droplets of the colloidal solution generated by an ultrasonic atomizer were carried by argon 1.0 L/min into a pretreated tubular furnace (1073 K). The evaporation of water in the droplets, the self-assembly and the reduction of GO were carried out in sequence in the tubular furnace. The fabricated 3-D CGR particles were collected by a Teflon membrane filter.

The photoanode of the DSSCs was prepared by coating TiO_2 paste onto an FTO glass substrate. TiO_2 nanoparticles (P25, Degussa), as-prepared 3-D CGR and GO were used as materials to prepare the TiO_2 paste, 3-D CGR/TiO_2 paste, and 3-D CGR/GR sheets/TiO_2 paste. The 3-D CGR/TiO_2 paste was prepared with a weight ratio of 0.003, while the amount of TiO_2 was fixed at 0.3 g. The prepared materials were dispersed into a mixture of acetic acid (0.05 mL), deionized water (0.25 mL), and ethanol (7 mL), in that order. Next, ethyl cellulose (0.15 g) as a binder and a solution of α-terpineol (1 mL) was added to the mixture while stirring. The 3-D CGR/GO sheets/TiO_2 paste was prepared by dispersing the GO sheets with a 3-D CGR/TiO_2 mixture (3-D CGR:GO sheets = 1:1), followed by the same mixing procedures. We chose the weight ratio of the GO sheets/3-D CGR was 1 because the highest PCE value was achieved with that ratio as shown in Supporting Information Figure S1 and Table S1.

The 3-D CGR-GO Sheets/TiO_2 composite paste was also prepared with a weight ratio of 0.003, while the amount of TiO_2 was fixed at 0.3 g. The various TiO_2 pastes were coated onto the FTO or GO modified FTO glass substrate to fabricate the photoanodes through the doctor blade to obtain approximately 15-μm thick films. After drying at room temperature for 30 min., the TiO_2 films were sintered at 423 K for 10 min, at 573 K for 20 min, and at 723 K for 40 min. During this annealing process, the GO sheets in the paste and on FTO glass were reduced to GR. Dye sensitization was performed by immersing the TiO_2 films in 0.4 mM N719 dye (Solaronix) ethanol solution for 24 h. The sensitized films were washed in ethanol and dried in air. Afterward, they were sandwiched and bonded with platinum-coated FTO counterelectrodes. The active area of the cells was 0.09 cm^2. The internal space of the cells was filled with a liquid electrolyte (An50, Solaronix).

The morphologies of the as-prepared GR modified FTO surface, 3-D CGR, and 3-D CGR/GR sheets/TiO_2 photoanode composite films were observed with FESEM (MLA 650 FEG, FEI). The photovoltaic properties of the DSSCs were measured with simulated AM 1.5 sunlight illumination with an output of 100 mW/cm^2. A solar simulator (L01, Peccell) with a 150 W Xenon lamp power supply was used as the light source. EIS was recorded under 1 Sun illumination over a frequency range of 0.05–10^5 Hz with an AC amplitude of 10 mV using Compactstat (Ivium).

Results and Discussion

To enhance the electron transport rate and reduce the charge-hole recombination at the interface between the FTO glass and TiO_2 particles, we coated GO sheets on the FTO using the LB technique. When the barrier moved toward the center of the trough, the GO sheets spread on the water surface were gathered, and the density of the sheets started to rise (I) seen in the surface pressure-area plot of Figure 1a. Because the barrier was closed to the FTO substrate, a gradual increase in the surface pressure was observed in region II. In the high surface pressure region (III), the sheets on the water surface collapsed and overlapped on the water during compression and thus, tended to be folded and over-packed. Therefore, we transferred the GO sheets on the FTO substrate at a surface pressure of 20 mN/m to get a uniform and close-packed sheet density without much overlap.

The morphology of the GO modified FTO is shown in Figure 1b. The lateral size of the sheets was in the micrometer scale; thus, one GO sheet can cover a number of FTO and TiO_2 nanoparticles. Although it was observed that a few GO sheets were not exfoliated (black region), most of the sheets were well dispersed and closely attached on the FTO glass without wrinkles as shown in the inset of Figure 1b. Because poor contact of the GO sheets with the FTO surface could

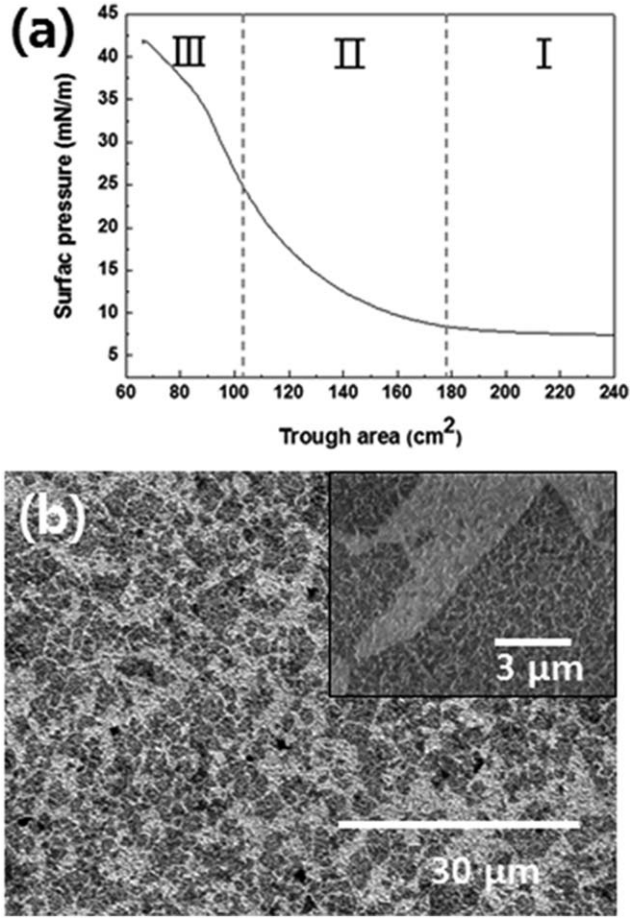

Figure 1. (a) Isothermal surface pressure-area plot during the LB deposition and (b) FESEM image of the modified FTO surface by GO sheets.

The inset is a high magnification image of closely attached GO sheets on the FTO glass without physical deformation.

significantly hinder the charge transport, GO coating with the LB technique is an alternative approach for reducing the recombination at the FTO/TiO_2 interface.[15]

Figure 2a shows the 3-D CGR particles prepared by the aerosol spray pyrolysis. The 3-D CGR has a spherical shape, and the average diameter of the particle is about 0.44 μm measured from the analysis results on particle size (Figure 2b). The D and G peaks in the Raman spectra in Supporting Information, Figure S2, show that the 3-D CGR was successfully reduced from the GO solution by aerosol spray pyrolysis. Yen et al. reported that 3-D CGR has small voids uniformly distributed inside the particles and a high compressive strength, which should be favorable for dye loading and infiltration of an electrolyte. Furthermore, the uneven shaped surface of the 3-D CGR can support a high specific surface area which can adsorb a number of dye molecules and TiO_2 nanoparticles.[4]

Cross-sectional SEM images of the photoanode pastes fabricated with TiO_2, 3-D CGR/TiO_2, and 3-D CGR/GR sheets/TiO_2 composite after the reduction and annealing are shown in Figure 3. Some of the 3-D CGR particles were marked with a doted circle line. In Figure 2a, the pure TiO_2 paste exhibited low porosity and roughness. Conversely, there were more pores in the electrode comprised of 3-D CGR/TiO_2 (Figure 2b) and in the 3-D CGR/GR sheets/TiO_2 composite (Figure 2c) that in the pure TiO_2 electrode. This enhanced porosity and roughness can be explained by the following reasons. When 3-D CGR particles were incorporated into the TiO_2, their presence in the paste was seen as black holes. In addition, Yang's group proved that GR incorporation increases the roughness factor in TiO_2 paste because of the gas released after the annealing process.[11] As a result, the incorporation of 3-D CGR and GR sheets into the TiO_2 enhanced the surface roughness of the photoanodes. The GR sheets were invisible in the cross-sectional images due to their thin layer thickness of 1–2 nm.

Figure 4 is a schematic illustration of the devices using the GR modified FTO and composite photoanodes. Three devices were fabricated with TiO_2, 3-D CGR/TiO_2, and 3-D CGR/GR sheets/TiO_2 pastes on the FTO surface without premodification by GR. They were, respectively, denoted as D1, D3, and D5, D2, D4 and D6 indicate devices comprised of GR modified FTO and TiO_2, 3-D CGR/TiO_2, and 3-D CGR/GR sheets/TiO_2 composite pastes, respectively. Considering their excellent conductivity and good contact with TiO_2, the incorporation of the 3-D CGR and GR sheets in the TiO_2 photoanode may benefit the charge transfer and performance of the

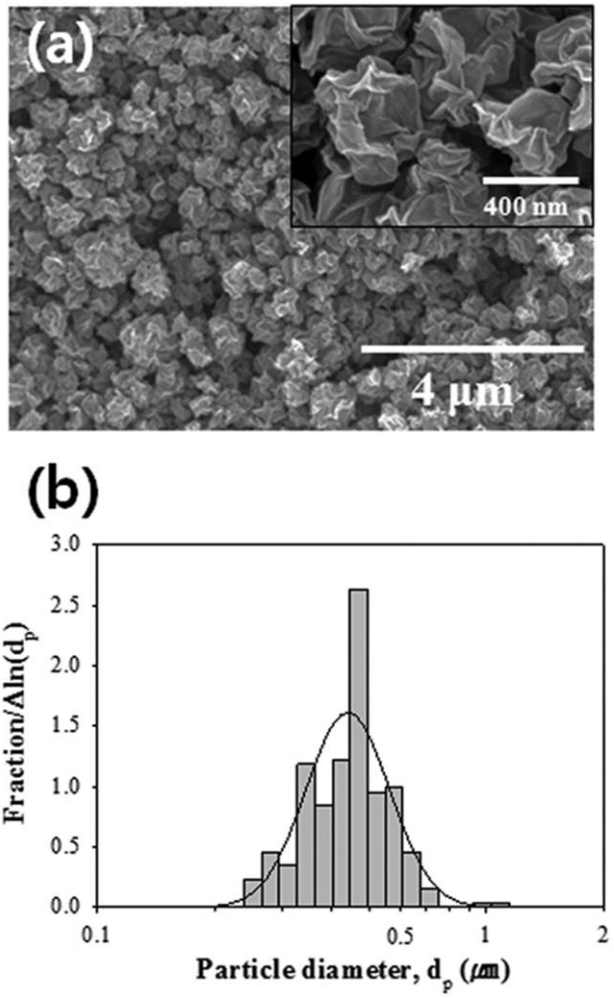

Figure 2. (a) FESEM images of the 3-D CGR particles. The inset is a high magnification image showing the accurate shape and size of the 3-D CGR. (b) Analysis results of the particle size for 3-D CGR prepared by aerosol spray pyrolysis.

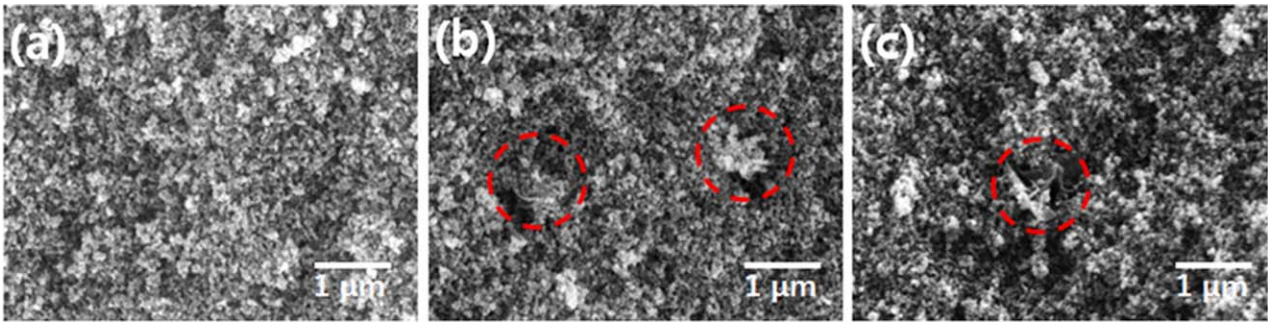

Figure 3. Cross-sectional FESEM images of (a) pure TiO_2, (b) 3-D CGR/TiO_2, and (c) 3-D CGR/GR sheets/TiO_2 photoanode pastes.

[Color figure can be viewed in the online issue, which is available at wileyonlinelibrary.com.]

DSSCs. It was observed that their film thickness was almost 15 μm without cracking or peeling after annealing at 723 K.

Using the composite films as the photoanode and FTO glasses, we fabricated DSSCs to evaluate their photovoltaic performance. The short-circuit current (J_{sc}), open-circuit voltage (V_{oc}), fill factor (FF), and PCE (η) are shown in Figure 5 and Table 1. A reference DSSC with only TiO_2 as the anode material and the original FTO had the following values: a J_{sc}, FF, and η of 11.7 mA/cm^2, 0.636, and 4.60%, respectively. After the incorporation of 3-D GR onto TiO_2 (D3), the J_{sc}, FF, and η values for the DSSC increased to 13.31 mA/cm^2, 0.652, and 5.49%, respectively, for which PCE was higher than that of D1. In the case of D5 which was fabricated with the 3-D CGR/GR sheets/TiO_2, the value of J_{SC} increased to 16.81 mA/cm^2, resulting in a PCE of 6.98%. These results shows that the 3-D CGR and GR sheets in the TiO_2 photoanode can significantly increase the PCE of DSSCs. DSSCs fabricated with the GR modified FTO substrates showed a similar PCE increment. The PCE values of the D2, D4, and D6 devices were 4.91, 6.72, and 7.20%, respectively, which were higher than those in the DSSCs without the GR modified FTO regardless of the photoanode types.

To understand the mechanism behind the performance improvement of the GR modification on the FTO and the incorporation of 3-D CGR and GR sheets into the TiO_2 paste, EIS measurements were taken under 1 Sun illumination. Figure 6 shows typical EIS Nyquist plots of DSSCs using the original (Figure 6a) or GR-coated (Figure 6b) FTO substrates at the open-circuit potential. The inset in Figure 6 means that the equivalent circuit was used to fit the DSSCs.[22] The small semicircle at the high frequency region in the Nyquist plot represents resistance R_1, caused by the charge transfer resistances at the counter Pt electrode/electrolyte interface. The large semicircle at the low frequency is attributed to the electron transfer resistance R_2 at the TiO_2/FTO and TiO_2/redox electrolyte interfaces.[15,23] R_s is the series resistance associated with other components such as the solution resistance, graphene coating, and so forth. The resistance values of EIS are summarized in Table 1. Because the same Pt counterelectrode and electrolyte were used in all the experiments, R_1 is not addressed in this study.

The R_2 values of the DSSCs based on the GR modified FTO substrates using TiO_2, 3-D CGR/TiO_2, and 3-D CGR/GR sheets/TiO_2 anode materials were 30.8, 22.2, and 17.0 Ω, respectively. These resistance values are, respectively, lower than those of the DSSCs based on the conventional FTO substrates using the same photoanodes. In a previous study, we reported that the GR sheet coating on the FTO substrates by the LB technique reduced the interface resistance between the FTO surface and TiO_2 paste and enhanced the charge-transfer rate, resulting in a higher efficiency of the DSSC.[15] However, when we compared the R_2 of the reference device D1 with those of D6, the resistance value was decreased to 49%. The reason for this dramatic reduction in R_2 is not simply explained by the GR coating on the FTO surface.

The charge transport resistance R_2 for D1 and D3 were 33.3 and 28.2 Ω, respectively. Because R_2 represents the charge transfer at the interface of the TiO_2/dye/electrolyte, these results indicate that 3-D CGR incorporated into the TiO_2 film can enhance the charge-transfer rate because graphene is an

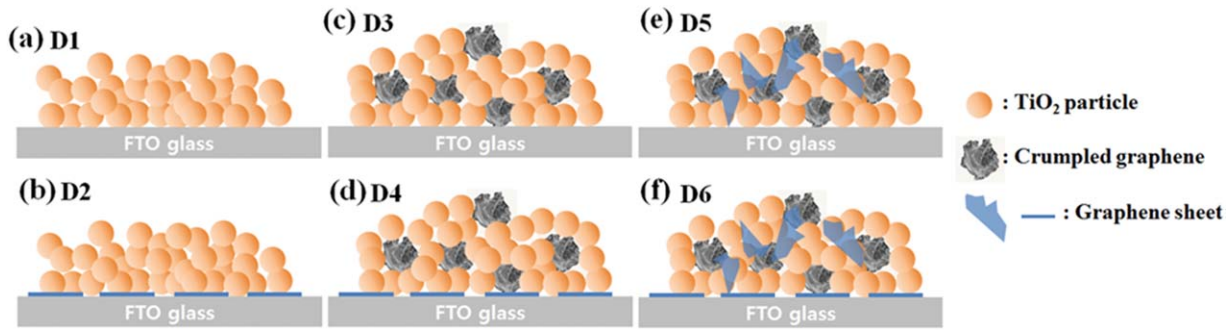

Figure 4. Schematic illustration of the devices using the original FTO glass with (a) pure TiO_2, (c) 3-D CGR/TiO_2, and (e) 3-D CGR/GR sheets/TiO_2 photoanode pastes. (b), (d), and (f) are, respectively, the devices using the pure TiO_2, 3-D CGR/TiO_2, and 3-D CGR/GR sheets/TiO_2 composite photoanodes with the GR modified FTO.

[Color figure can be viewed in the online issue, which is available at wileyonlinelibrary.com.]

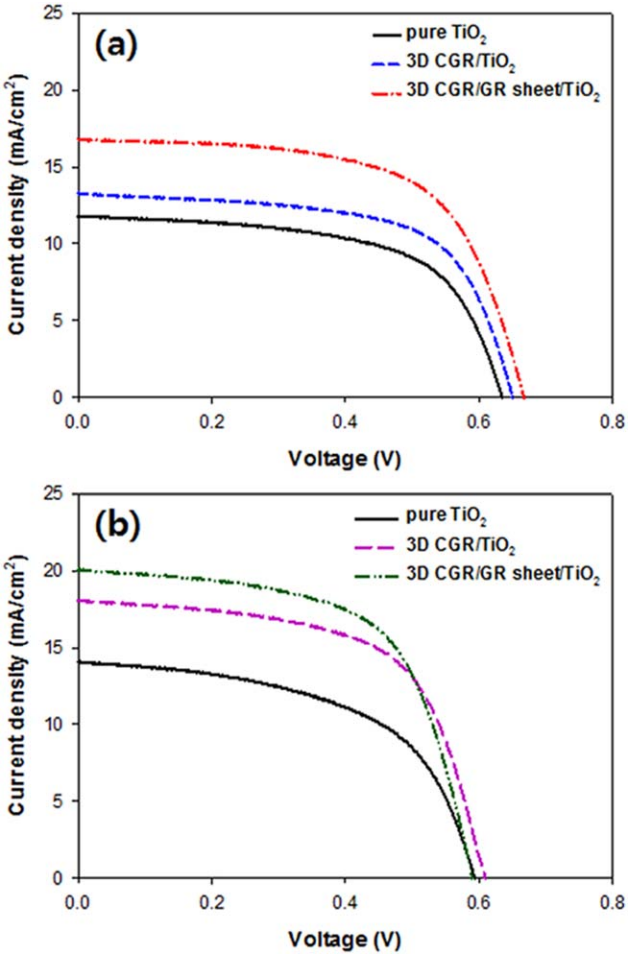

Figure 5. I-V curves of the DSSCs with pure TiO_2, 3-D CGR/TiO_2, and 3-D CGR/GR sheets/TiO_2 photoanode pastes using (a) conventional and (b) graphene modified FTO glass substrates under AM 1.5 sunlight illumination with an output of 100 mW/cm^2.

[Color figure can be viewed in the online issue, which is available at wileyonlinelibrary.com.]

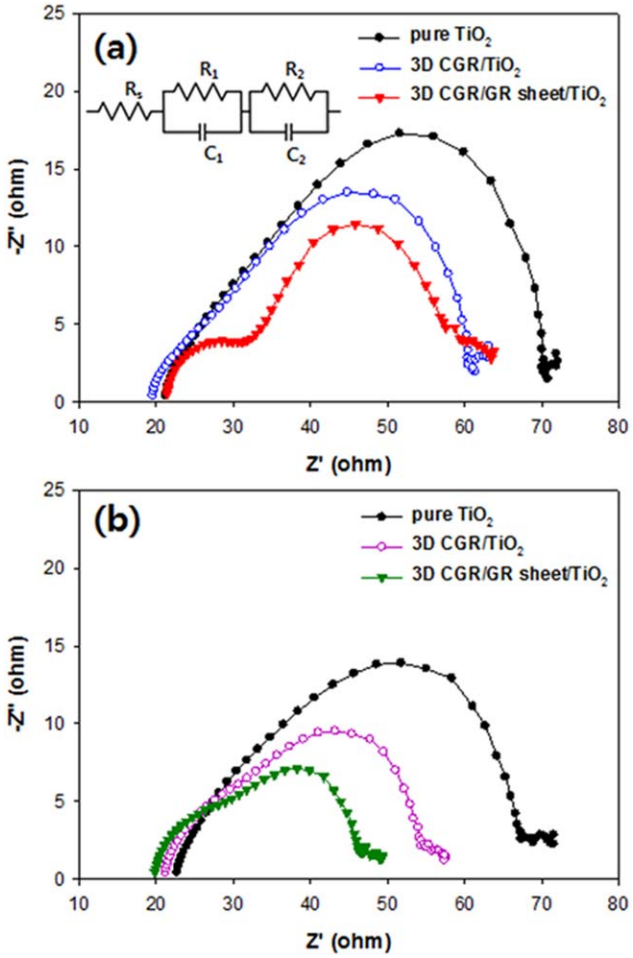

Figure 6. EIS spectra of the DSSCs using (a) conventional and (b) graphene modified FTO glass substrates.

The inset shows the equivalent circuit. [Color figure can be viewed in the online issue, which is available at wileyonlinelibrary.com.]

excellent electron carrier.[17] The other reason for the reduction of R_2 might be the dye loading capability of 3-D CGR. The high specific surface area and good adhesion for TiO_2 materials of the 3-D CGR particles can adsorb a great number of dye molecules and produce more photogenerated electrons than that of conventional DSSC devices. In addition, the R_2 for Device 5 with the 3-D CGR/GR sheets/TiO_2 photoanode decreased to 25.8 Ω, which corresponds to the improved conversion efficiency. When a GR sheet exists in a network of TiO_2 particles, electrons can be transported from TiO_2 to graphene because the conduction band of TiO_2 (−4.2 eV vs. vacuum) is more positive than the work function of GR (−4.4 eV vs. vacuum).[9,11] Thereby, the introduced 2-D GR sheets covered with TiO_2, CGR, and dye can act as a conductive bridge connecting the dye-TiO_2, TiO_2-TiO_2, and TiO_2−3-D CGR particles to increase the charge transport and suppress recombination in the photoanode. The change in the resistance R_2 by the incorporation of the 3-D CGR and GR sheets in TiO_2 is in agreement with the electron lifetime evolution. The maximum frequencies (ω_{max}) for D1, D3, and D5 were 45.4, 33.7, and 13.9 Hz, respectively. Because the lifetime of electrons in the film (τ_e) can be calculated from the inverse ω_{max} ($\tau_e = 1/2\pi\omega_{max}$); a decreased ω_{max} indicates that the photogenerated electrons from the dye molecules can move a longer distance with a reduced rate of charge-hole recombination due to the 3-D CGR and GR sheets incorporated into the network of

Table 1. Performance Parameters of the DSSCs with Different Photoanodes and FTO Glass Substrates

Device	Jsc [mA/cm^{-2}]	Voc [V]	FF	PCE [%]	Rs [Ω]	r2 [Ω]	Photoanode	GR on FTO
D1	11.77	0.636	63.36	4.60	21.2	33.3	TiO_2	X
D2	14.07	0.597	59.72	4.91	22.7	30.8	TiO_2	○
D3	13.31	0.652	65.65	5.49	19.6	28.2	3D CGR/TiO_2	X
D4	18.07	0.608	62.89	6.72	21.2	22.2	3D CGR/TiO_2	○
D5	16.81	0.667	63.16	6.98	21.4	25.8	3D CGR/GR sheets/TiO_2:	X
D6	20.02	0.590	62.19	7.20	19.8	17.0	3D CGR/GR sheets/TiO_2	○

TiO_2 particles. Therefore, using a GR modified FTO and 3-D CGR/GR sheets/TiO_2 composite offer a novel and efficient approach to achieve a higher performance in DSSCs.

Conclusions

We presented a high performance DSSC through the combination of a GR modified FTO and a composite photoanode consisting of 3-D CGR/GR sheets/TiO_2. The experimental results show that the PCE of the DSSC increased because of the following: (1) the GR coating on FTO surface reduced the charge recombination at the interface between the FTO and TiO_2 pastes, (2) the 3-D CGR particles adsorbed a great number of dye molecules and enhanced the production of photogenerated electrons due to their high specific surface area and rapid electron transport, and (3) 2-D GR sheets covered with dye/TiO_2/3-D CGR particles acted as a conducting bridge between the structured materials because the sheets supported rapid electron transport in the photoandoe. Consequently, the final PCE of the DSSC with the GR modification on the FTO and 3-D CGR/GR sheets/TiO_2 composited paste was remarkably increased from 4.6 to 7.2% which was 56% higher than that of the conventional DSSC.

Acknowledgment

This research was supported by the Basic Research Project of the Korea Institute of Geoscience and Mineral Resources (KIGAM), funded by the Ministry of Science, ICT and Future Planning.

Literature Cited

1. O'Regan B, Grätzel M. A low-cost, high-efficiency solar cell based on dye-sensitized colloidal TiO_2 films. *Nature*. 1991;353:737–740.
2. Grätzel M. Recent advances in sensitized mesoscopic solar cells. *Acc Chem Res*. 2009;42:1788–1798.
3. Yu JG, Fan JJ, Lv KL. Anatase TiO_2 nanosheets with exposed (001) facets: improved photoelectric conversion efficiency in dye-sensitized solar cells. *Nanoscale*. 2010;2:2144–2149.
4. Yen MY, Hsiao MC, Liao SH, Liu PI, Tsai HM, Ma CC, Pu NW, Ger MD. Preparation of graphene/multi-walled carbon nanotube hybrid and its use as photoanodes of dye-sensitized solar cells. *Carbon*. 2011;49:3597–3606.
5. Park NG, Schlichthörl G, Van de Lagemaat J, Cheong HM, Mascarenhas A, Frank AJ. Dye-sensitized TiO_2 solar cells: structural and photoelectrochemical characterization of nanocrystalline electrodes formed from the hydrolysis of TiCl4. *J Phys Chem B*. 1999;103:3308–3314.
6. O'Regan B, Durrant JR, Sommeling PM, Bakker NJ. Influence of the $TiCl_4$ treatment on nanocrystalline TiO_2 films in dye-sensitized solar cells. 2. Charge density, band edge shifts, and quantification of recombination losses at short circuit. *J Phys Chem C*. 2007;111:14001–14010.
7. Ito S, Murakami TN, Comte P, Liska P, Grätzel C, Nazeeruddin MK, Grätzel M. Fabrication of thin film dye sensitized solar cells with solar to electric power conversion efficiency over 10%. *Thin Solid Films*. 2008;516:4613–4619.
8. Fang X, Li M, Guo K, Liu X, Zhu Y, Sebo B, Zhao X. Graphene-compositing optimization of the properties of dye-sensitized solar cells. *Sol Energy*. 2014;101:176–181.
9. Chen T, Hu W, Song J, Guai GH, Li CM. Interface functionalization of photoelectrodes with graphene for high performance dye-sensitized solar cells. *Adv Funct Mater*. 2012;22:5245–5250.
10. Tang YB, Lee CS, Xu J, Lui ZT, Chen ZH, He Z, Cao YL, Yuan G, Song H, Chen L, Luo L, Cheng HM, Zhang WJ, Bello I, Lee ST. Incorporation of graphenes in nanostructured TiO_2 films via molecular grafting for dye-sensitized solar cell application. *ACS Nano*. 2010;4:3482–3488.
11. Yang N, Zhai J, Wang D, Chen Y, Jiang L. Two-dimensional graphene bridges enhanced photoinduced charge transport in dye-sensitized solar cells. *ACS Nano*. 2010;2:887–894.
12. Luo J, Jang HD, Huang J. Effect of sheet morphology on the scalability of graphene-based ultracapacitors. *ACS Nano*. 2013;2:1464–1471.
13. Chen L, Zhou Y, Tu W, Li Z, Bao C, Dai H, Yu T, Liu J, Zou Z. Enhanced photovoltaic performance of a dye-sensitized solar cell using graphene–TiO_2 photoanode prepared by a novel in situ simultaneous reduction-hydrolysis technique. *Nanoscale*. 2013;5:3481–3485.
14. Wang X, Zhi LJ, Mullen K. Transparent, conductive graphene electrodes for dye-sensitized solar cells. *Nano Lett*. 2008;8:323–327.
15. Roh KM, Jo EH, Chang H, Han TH, Jang HD. High performance dye-sensitized solar cells using graphene modified fluorine-doped tin oxide glass by Langmuir–Blodgett technique. *J Solid State Chem*. 2015;224:71–75.
16. Cote LJ, Kim F, Huang J. Langmuir−Blodgett assembly of graphite oxide single layers. *J Am Chem Soc*. 2009;131:1043–1049.
17. Jang HD, Jo EH, Chang H, Roh KM. Incorporation of 3D crumpled graphene in nanostructured TiO_2 films. *Mater Lett*. 2015;142:304–307.
18. Luo J, Jang HD, Sun T, Xiao L, He Z, Katsoulidis AP, Kanatzidis MG, Gibson JM, Huang J. Compression and aggregation-resistant particles of crumpled soft sheets. *ACS Nano*. 2015;5:8943–8949.
19. Luo J, Kim J, Huang J. Material processing of chemically modified graphene: some challenges and solutions. *Acc Chem Res*. 2013;46:2225–2234.
20. Chang H, Jang HD. Controlled synthesis of porous particles via aerosol processing and their applications. *Adv Powder Technol*. 2014;25:32–42.
21. Kim SK, Chang H, Choi JW, Huang J, Jang HD. Aerosol processing of graphene and its application to oil absorbent and glucose biosensor. *Kona Powder Part J*. 2014;31:111–125.
22. Xu H, Tao X, Wang DT, Zheng YZ, Chen JF. Enhanced efficiency in dye-sensitized solar cells based on TiO_2 nanocrystal/nanotube double-layered films. *Electrochim Acta*. 2010;55:2280–2285.
23. Xi JT, Zhang QF, Park K, Sun YM, Cao GZ. Enhanced power conversion efficiency in dye-sensitized solar cells with TiO_2 aggregates/nanocrystallites mixed photoelectrodes. *Electrochim Acta*. 2011;56:1960–1966.
24. Hummers WS, Offenman RE. Preparation of graphitic oxide. *J Am Chem Soc*. 1958;80:1339–1339.

Manuscript received June 29, 2015, and revision received Sep. 22, 2015.